LETTERS

Breakdown of the Bardeen–Cooper–Schrieffer ground state at a quantum phase transition

R. Jaramillo[1], Yejun Feng[1,2], J. C. Lang[2], Z. Islam[2], G. Srajer[2], P. B. Littlewood[3], D. B. McWhan[4] & T. F. Rosenbaum[1]

Advances in solid-state and atomic physics are exposing the hidden relationships between conventional and exotic states of quantum matter. Prominent examples include the discovery of exotic superconductivity proximate to conventional spin and charge order[1,2], and the crossover from long-range phase order to preformed pairs achieved in gases of cold fermions[3–5] and inferred for copper oxide superconductors[5]. The unifying theme is that incompatible ground states can be connected by quantum phase transitions. Quantum fluctuations about the transition are manifestations of the competition between qualitatively distinct organizing principles[6,7], such as a long-wavelength density wave and a short-coherence-length condensate. They may even give rise to 'protected' phases, like fluctuation-mediated superconductivity that survives only in the vicinity of an antiferromagnetic quantum critical point[8,9]. However, few model systems that demonstrate continuous quantum phase transitions have been identified, and the complex nature of many systems of interest hinders efforts to more fully understand correlations and fluctuations near a zero-temperature instability. Here we report the suppression of magnetism by hydrostatic pressure in elemental chromium, a simple cubic metal that demonstrates a subtle form of itinerant antiferromagnetism[10–16] formally equivalent to the Bardeen–Cooper–Schrieffer (BCS) state in conventional superconductors. By directly measuring the associated charge order in a diamond anvil cell at low temperatures, we find a phase transition at pressures of ~10 GPa driven by fluctuations that destroy the BCS-like state but preserve the strong magnetic interaction between itinerant electrons and holes. Chromium is unique among stoichiometric magnetic metals studied so far in that the quantum phase transition is continuous, allowing experimental access to the quantum singularity and a direct probe of the competition between conventional and exotic order in a theoretically tractable material.

Chromium is a b.c.c. crystal that forms a spin-density wave (SDW) below a Néel temperature of $T_N = 311$ K. This weak-coupling ground state of electron–hole pairs is described by a BCS-like exponential expression for the magnetic moment, μ, of the form $\mu(T=0) \propto \exp(-1/\lambda)$, where the coupling constant, λ, can be tuned by application of pressure, P, and chemical doping. The SDW is modulated by a wavevector, **Q**, of magnitude Q (in units of $2\pi/a$, where a is the lattice constant), which is selected by the nesting condition and is slightly incommensurate with the crystal lattice (Fig. 1, inset). The SDW is accompanied by an itinerant charge density wave (CDW), which is modulated by 2**Q** and is thought of as the second harmonic of the SDW[17]. This harmonic relationship between spin and charge is consistent with the $I_{CDW} \propto I_{SDW}^2 \propto \mu^4$ scaling (where I is scattering intensity), observed as a function of both temperature[18] and pressure[14].

Tuning the magnetism towards the quantum phase transition using pressure while directly measuring the charge and spin order parameters is the conceptually preferred route to studying the quantum critical regime. By using P as our tuning variable, we avoid the complications of chemical doping, such as variable band filling and substitutional disorder, that may be significant at the critical point. Our high-resolution X-ray diffraction technique provides a direct measurement of the order parameters and a view into the microscopic world of nested electron–hole pairs. However, the

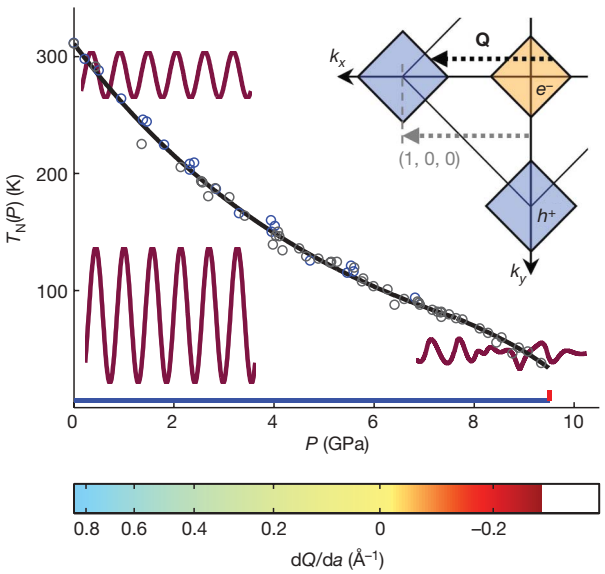

Figure 1 | Phase diagram and Brillouin zone schematic for magnetism in chromium. Phase diagram shows $T_N(P)$; grey points are determined from our data using the mean-field relation $T_N \propto I_{CDW}^{1/4}(T=0)$, blue points are determined from resistivity measurements of T_N (ref. 11; also see refs 13, 14 and Fig. 4 for a discussion of pressure scales) and black line is a guide to the eye. Blue and red lines indicate experimental cuts (see Supplementary Information for data collected along the red trajectory). The colour bar charts the change in SDW wavevector, Q, with pressure (at $T < 8$ K) as measured by dQ/da, the derivative with respect to chromium lattice constant. The quantum critical regime is marked by both a deviation from the exponentially tuned BCS ground state and an unexpected changed in the sign of dQ/da. The three cartoons are proposed representations of the density-wave order parameter in three regimes. At low T and low P, the order-parameter amplitude is large and highly ordered. At high T and low P, the amplitude is reduced before being cut off by a first-order phase transition. At low T and high P, the amplitude is further reduced and the transition is driven by transverse fluctuations (not drawn to scale). Inset, schematic of the first Brillouin zone, showing the incommensurate wavevector, **Q**, connecting the nested sections of Fermi surface that are eliminated in the magnetic phase by the formation of an exchange-split energy gap[16].

[1]The James Franck Institute and Department of Physics, The University of Chicago, Chicago, Illinois 60637, USA. [2]The Advanced Photon Source, Argonne National Laboratory, Argonne, Illinois 60439, USA. [3]Cavendish Laboratory, University of Cambridge, Cambridge CB3 OHE, UK. [4]Department of Physics, Massachusetts Institute of Technology, Cambridge, Massachusetts 02139, USA.

experimental challenges are daunting. The pressure required to drive the transition is of the order 100,000 atm, necessitating the use of diamond-anvil-cell and synchrotron X-ray diffraction techniques. Tracking just the CDW order parameter into the quantum critical regime requires measuring satellite diffraction peaks that are nearly 10^{10} times weaker than the lattice Bragg reflections in high-quality single-crystal samples at high pressure and low temperature.

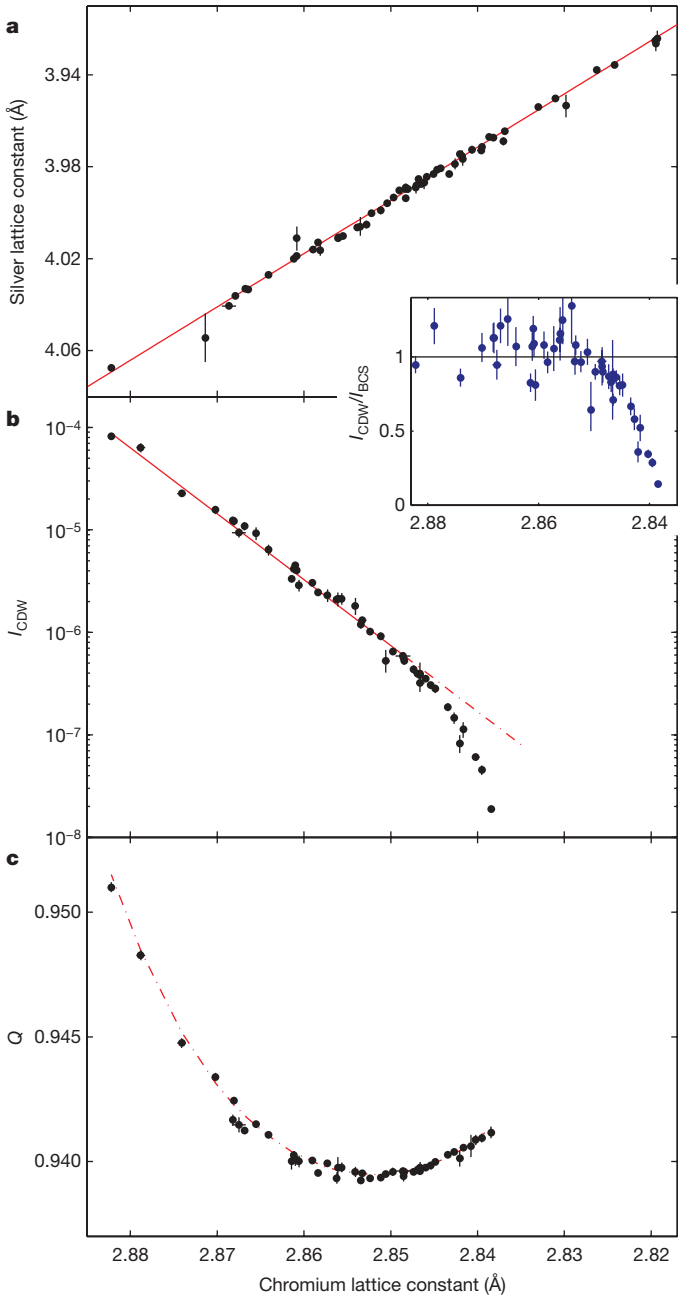

Figure 2 | Structure, CDW intensity and wavevector *Q* for $T < 8$ K. **a**, Variation of the silver lattice constant over a wide range of chromium lattice constant. The high-fidelity linear fit rules out a significant first-order transition in the critical pressure range. **b**, Normalized CDW intensity, I_{CDW}, summed over all three domain types (see Methods); for $a = 2.8348$ Å, we have established an upper bound on I_{CDW} of 5.9×10^{-9} (not plotted). The exponential fit to the data in the non-critical regime is shown in red. Inset, fractional deviation of I_{CDW} from the mean-field ground state, I_{BCS}, determined from the exponential fit in **b**. **c**, Magnitude, *Q*, of the SDW wavevector, showing an unexpected upturn in the critical pressure range. This contrasts with the gently decreasing dependence on pressure in the non-critical regime. The red curve is a polynomial fit used to generate d*Q*/d*a* as presented in Fig. 1. Error bars on lattice constants and *Q* represent s.d.; error in I_{CDW} is s.e.m.

In Fig. 2, we present X-ray diffraction measurements of the CDW order parameter, the magnitude of magnetic wavevector, *Q*, and the chromium lattice in the quantum critical regime. Our data establish the existence of a continuous, antiferromagnetic quantum phase transition in this stoichiometric model system. In Fig. 2a, we plot the lattice constant of silver, our pressure calibration, over a wide range of chromium lattice constant corresponding to $0 < P < 14.5$ GPa. The continuous evolution of the chromium lattice throughout this pressure range precludes the existence of a significant first-order quantum phase transition, as has been seen in direct order-parameter measurements for every other stoichiometric, itinerant magnet studied so far[19].

The evolution of the CDW order parameter through this pressure range is presented in Fig. 2b, where we plot the CDW diffraction intensity, I_{CDW} (see Methods), as a function of chromium lattice constant. I_{CDW} decreases by more than two orders of magnitude between 0 and 7 GPa, where it is faithfully described by an exponential dependence on *P* (refs 14, 15). Above 7 GPa, the intensity falls away from this mean-field expectation, and by 9.5 GPa it is nearly one order of magnitude weaker than the extrapolated exponential fit (Fig. 2, inset). At the highest measured pressure, the magnetic moment satisfies $\mu/\mu_0 = (I_{CDW}/I_{CDW,0})^{1/4} = 0.12$, where $\mu_0 = 0.41\mu_B$ is the root-mean-square ordered moment at ambient pressure and low temperature, μ_B is the Bohr magneton and $I_{CDW,0}$ is the CDW diffraction intensity at zero pressure and base temperature. This should be compared with the value $\mu/\mu_0 = 0.27$, which obtains at the weakly first-order Néel transition at ambient pressure[20]. The antiferromagnetic phase transition therefore crosses from first-order to second-order behaviour as we pass from the thermal to the quantum regime.

The deviation of I_{CDW} from the weak-coupling ground state is accompanied by an unexpected upturn in *Q* (Fig. 2c and the colour bar in Fig. 1). In the exponentially tuned regime, *Q* decreases slowly with pressure (by sharp contrast with the response to chemical doping[15]) and appears to level off for $P > 4$ GPa, providing evidence for a rigid band structure in chromium at this pressure scale[14,15]. The upturn in *Q* above 7 GPa signals the start of a new relationship between pressure, magnetism and band structure.

To understand the origin of this behaviour, we first turn to a mean-field theory that is appropriate for the system at ambient pressure. In the absence of fluctuations, the free energy of the magnetic state can be written as

$$F = \frac{1}{2}a_0|\psi_0|^2 + \frac{1}{4}b_0|\psi_0|^4 + \frac{1}{2}\xi_0^2(\nabla\psi_0)^2 + \frac{1}{2}e_0|\psi_0|^2|\nabla\phi - \mathbf{q}|^2 + f_0|\psi_0|^4\cos(2\phi) \quad (1)$$

where $|\psi_0|e^{i\phi}$ is the SDW order parameter, $\mathbf{q}$ is the nesting vector as determined by the band structure and the coefficients a_0, b_0, …, f_0 characterize the SDW state. The final two terms allow $Q = |\nabla\phi|$ to vary from $q = |\mathbf{q}|$, the first expressing the cost of repopulating the Brillouin zone to accommodate $Q \neq q$, and the second reflecting the coupling of the CDW to the lattice.

The different ψ_0 dependences of the final two terms equation (1) allow us to distinguish between the various mechanisms that affect *Q*. In Fig. 3a, we show *Q* as a function of the ordered moment $\mu \cong |\psi_0|$ for both the temperature- and the pressure-driven phase transitions. In the thermal case, *Q* varies rapidly when μ is strong ($\mu \approx \mu_0$), but levels off for $\mu/\mu_0 < 0.6$. This identifies $0.6 < \mu/\mu_0 < 1$ as the regime in which the final two terms in equation (1) are in competition; for smaller magnetic moments, the quartic term is too weak to affect *Q*. For the pressure-driven transition, the regime $0.6 < \mu/\mu_0 < 1$ is likewise characterized by a monotonic change of *Q* with μ, with *Q* levelling off as the magnetism is further suppressed, before suddenly increasing for $\mu/\mu_0 < 0.3$. This upturn on the approach to the critical regime cannot be explained by competition between the two *Q*-dependent terms in equation (1). We measured the temperature dependence of *Q* at $P = 9.5$ GPa and found it to be constant up to $T = 15$ K (see experimental cut in Fig. 1 and data in Supplementary Information), ruling out the effects of finite

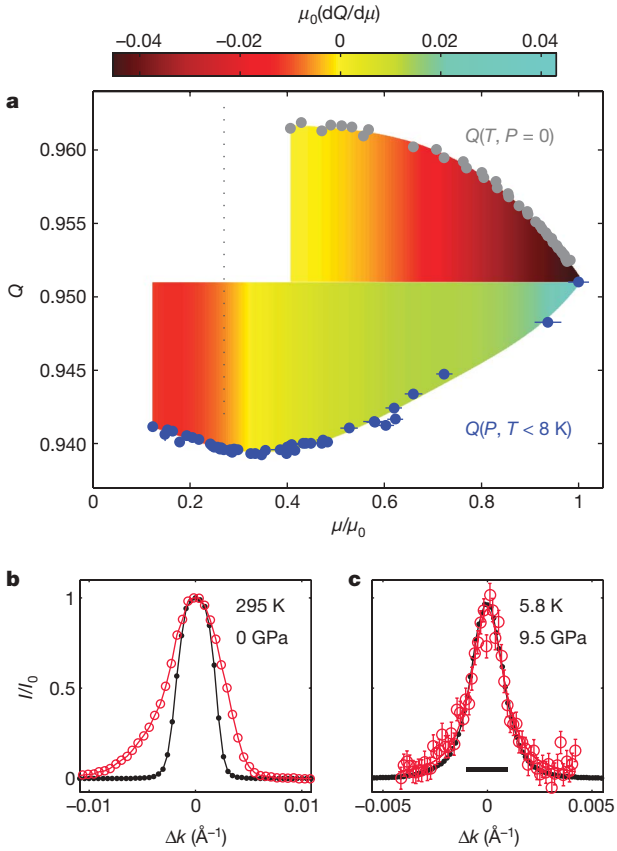

Figure 3 | Dependence of Q on order parameter and band structure in the classical and quantum regimes. **a**, Variation of Q with ordered moment, μ, for both temperature- and pressure-driven phase transitions. Colour maps represent $\mu_0(dQ/d\mu)$ determined by smooth polynomial fits to the data in the thermal (upper colour map) and quantum (lower colour map) cases. Data for $Q(T, P = 0)$ are taken from the literature[18,29] and $\mu(T)$ is established by neutron diffraction[20]. For our high-pressure measurements, μ is calculated using the $\mu \propto I_{CDW}^{1/4}$ mean-field relationship. The vertical dotted line marks the level at which the magnetic order is cut off by a weak first-order phase transition at the ambient pressure Néel temperature. Error bars on Q represent s.d.; error in μ is s.e.m. **b**, **c**, Longitudinal CDW (red) and lattice (black) diffraction line shapes in the thermal (**b**) and quantum (**c**) critical regimes. All scans are normalized to peak intensity, and error bars are s.e.m. In the thermal case, the lattice and CDW diffraction peaks are $(2, 0, 0)$ and $(4 - 2Q, 0, 0)$, and in the quantum case they are $(2, 1, 1)$ and $(4 - 2Q, 1, 1)$; these reflections are chosen to optimize the structure factor in the critical regime[15]. Asymmetric broadening of the CDW line shape near the thermal transition reflects imperfect Fermi surface nesting at high temperature[15]. By contrast, the CDW line shape near the quantum transition is instrument-limited, indicating that the Fermi surface nesting remains excellent. Instrument resolution (FWHM) is indicated by the black bar; the instrument-limited line shape places a lower bound of 2,000 Å on the longitudinal CDW correlation length.

temperature as an explanation. Although we cannot rule out changes to the underlying band structure, a non-monotonic evolution of q with a reduction in a of only 1.5% seems unlikely, as is a coincidence of the upturn in Q with the approach to the critical regime. We conclude that equation (1) is inadequate for describing the evolution of Q in the quantum critical regime, and instead require an expression that goes beyond the mean-field assumption to include a full set of coupled fluctuation terms at second order in ψ_0.

Although Q responds to changes in q, it does not reflect more subtle changes to the band structure that can affect the magnetism. The nesting feature of the paramagnetic band structure leads to a peak in the wavevector (k)-dependent non-interacting susceptibility, $\chi_0(k)$, at $k = q$. For ideal nesting (perfectly flat Fermi surfaces) this peak diverges logarithmically and the weak-coupling ground state is stable for arbitrarily small coupling constant, λ. As a consequence, a_0, the

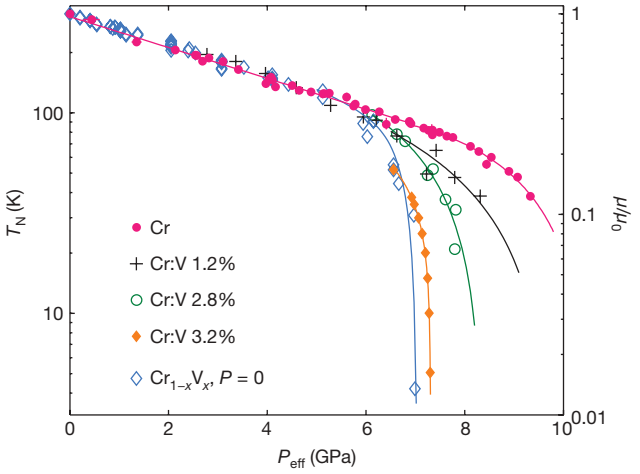

Figure 4 | Disparate routes to quantum criticality. The effects of pressure and vanadium doping on the magnetic ordered moment, μ (or T_N), are plotted together to reveal a family of antiferromagnetic quantum phase transitions. By compressing pure chromium into the critical regime, we are able to distinguish the effects of pressure and chemical doping on the magnetism (compare with fig. 4 in ref. 13). Data for $Cr_{1-x}V_x(P = 0)$ and results for $x = 1.2\%$, 2.8% and 3.2% under pressure are taken from the literature[13–15,30]. All curves are determined from measurements of T_N except for our scattering data, for which the measured quantity is $I_{CDW} \propto \mu^4$. Pressure and doping are related by 2.05 GPa = 1% V, set by the collapse of the data for $I_{CDW}^{1/4}(P < 7\ \text{GPa}, x = 0)$ and $T_N(P = 0, x < 2.5\%)$ onto the same exponential curve. Data are plotted against effective pressure, $P_{eff} = P + (2.05\ \text{GPa})100x$, the sum of applied and chemical pressure. The reported pressure scale for the data for vanadium doping of 1.2% and 2.8% has been reduced by a factor of 1.2. This reduction factor collapses the reported $T_N(P, x = 0)$ curve onto our measured $I_{CDW}^{1/4}(P, x = 0)$ curve, where the former was measured by the same group using the same experimental technique as here for $T_N(P, x = 1.2\%)$ and $T_N(P, x = 2.8\%)$ (refs 11, 14, 30). Disorder destabilizes the BCS ground state but, unlike for pure chromium, does not permit deconvolution of the physics of fluctuations, impurity scattering and Fermi surface warping.

quadratic coefficient in equation (1), vanishes non-analytically at a critical mean-field pressure P_{C0} (in fact $a_0^{BCS} \propto \exp[1/(P - P_{C0})]$) and the correlation length, $\xi = \xi_0(a_0)^{-1/2}$, diverges so rapidly that quantum fluctuations are irrelevant in the BCS theory. Under realistic nesting conditions, the peak at $\chi_0(k = q)$ is finite and the weak-coupling theory is more limited in scope. The critical point now occurs at a non-zero coupling constant, λ_C, and the conventional Ginzburg–Landau behaviour is recovered: $a_0^{MF} \propto P - P_{C1}$. Hence, a renormalized transition (but one still mean-field-like in this approximation) at a lower critical pressure, $P_{C1} < P_{C0}$, is expected. Crucially, the correlation length vanishes as a power law and quantum fluctuations will play a role close to the true critical point.

The nesting condition is characterized by the warping of the magnetic Fermi surfaces away from being ideally flat. This warping is measured by the longitudinal CDW line scans presented in Fig. 3. Close to the ambient-pressure Néel transition, the CDW line shapes[15] are broad and asymmetric (Fig. 3b). The broadening is a straightforward result of thermal melting of the density wave[18], and the asymmetry results from warped Fermi surfaces, which lead to an asymmetric set of low-energy excitations away from the equilibrium Q value. The longitudinal CDW line scans remain broadened even at 5 K at ambient pressure, where the (deconvolved) CDW full-width at half-maximum (FWHM) is 1×10^{-3} Å^{-1}, pointing to the presence of longitudinal CDW excitations ($\Delta Q/Q = 0.02\%$) even at this low temperature. By contrast, a longitudinal CDW line scan made at 9.5 GPa and 6 K (Fig. 3c) shows no signs of broadening to within 3×10^{-4} Å^{-1}. Q is stiffer in the longitudinal direction at $T = 6$ K and $P = 9.5$ GPa than at 5 K and 0 GPa, indicating an improvement in the nesting condition under pressure. We therefore consider the quantum phase transition not to

be a failure of nesting, but rather to be a crossover into a regime in which weak-coupling theory is invalid despite the existence of a well-defined nesting feature[21].

To better understand this crossover, in Fig. 4 we consider the family of antiferromagnetic quantum phase transitions that is related by varying applied pressure and vanadium doping. It is immediately apparent that pressure and doping cannot be brought into a one-to-one correspondence throughout the phase diagram. This suggests different microscopic roles for these two tuning variables, consistent with the qualitatively distinct dependences Q has on pressure and doping[15]. The effect of chemical doping on the nested band structure is underscored by recent results[22] that suggest multiple $\mathbf{Q}$ vectors in highly-doped Cr:V, where no such evidence exists for the pure system.

We can discuss these differences within a single conceptual framework by considering the relevant length scales on which the ground state deviates from the weak-coupling prediction. The electron–hole-pair coherence length for the parent system (pure chromium at zero temperature and pressure) is $\xi \approx v_F/\Delta = 35$ Å, where v_F is the Fermi velocity. In general, weak-coupling theory should become more appropriate as the gap, Δ, is suppressed: to escape the weak-coupling ground state, we require a cut-off length scale beyond which pair coherence breaks down. For doping-driven transitions, both impurity scattering and changes to the nesting condition can provide this length scale, and both agree qualitatively with the systematic trend in the critical pressure with alloying. The observation of non-mean-field scaling in the excess magnetic resistivity at the pressure-driven quantum phase transition in Cr:V 3.2% points to the importance of fluctuations in the quantum regime[13]. The difficulty lies in relating this transport signature of quantum criticality to the requisite cut-off length scale, and in distinguishing between multiple sources for this cut-off. Importantly, and by contrast, this complication is absent for pure chromium under pressure, where fluctuations provide the most natural explanation for a breakdown length scale. This highlights the advantages of studying the parent system with a clean tuning parameter, including the need for magnetotransport and thermodynamic measurements at the dissolution of the BCS state, and provides access to a regime of longer pair coherence lengths, where lower-energy fluctuations may be relevant at the quantum phase transition.

Pure chromium deviates from the weak-coupling ground state for $P > 7.3$ GPa, at which pressure $\Delta < 19$ meV and $\xi > 125$ Å. By 9.5 GPa, the respective values are 9 meV and 260 Å. The resolution-limited CDW line scan (Fig. 3c) rules out both Fermi surface distortion and longitudinal fluctuations as candidates to disrupt the ground state on this length scale. We therefore posit that fluctuations transverse to $\mathbf{Q}$ on a length scale of several hundred angstroms render the weak-coupling theory inappropriate for $P > 7.3$ GPa. We do in fact observe line-shape broadening in the transverse direction consistent with such fluctuations, but cannot make a definitive claim given the crystal-lattice mosaic of individual domains. Similar anisotropic correlations are often found in three-dimensional systems such as quantum critical $CeCu_{6-x}Au_x$ (ref. 23) and CDW systems with quasi-one-dimensional electronic structure[24,25], and the probability of anisotropic fluctuations in chromium speaks to the quasi-one-dimensional dispersion relation of carriers at the highly nested Fermi surfaces. At the high pressures of our experiment, the SDW remains in the transverse phase for all T (ref. 14), leading to the possibility of transverse fluctuations of spin-polarization (*S*-domain[10]) correlation volumes.

This work addresses a question that is germane to the study of ordered electrons in general, namely that of how a single ground state emerges at a quantum phase transition in a system with multiple energy scales[26]. It is understood that, despite the weak-coupling density-wave ground state, chromium possesses a hierarchy of energy scales that bridge the traditional boundary between weak and strong coupling[15]. Here we show that the feature responsible for this strong-coupling phenomenology, namely the highly nested Fermi surfaces, survives into the quantum critical regime. It is therefore plausible that bosonic electron–hole pairs remain viable after the long-range phase coherence is destroyed. This presents the possibility that phenomena more typically associated with strongly coupled systems, such as local phase segregation or condensation of bosonic pairs, may be possible high-pressure ground states in this simplest of model systems. The crossover to a Bose–Einstein condensate of short-coherence-length pairs, observed in both cold atoms[3–5] and dimerized magnetic insulators[27], might be an organizing principle for a wider range of systems.

METHODS SUMMARY

We performed direct measurement of the CDW order parameter using monochromatic X-ray diffraction at insertion device beamline 4-ID-D of the Advanced Photon Source, Argonne National Laboratory. A silicon double-bounce monochromator was used to provide 20,000-keV X-rays, and a pair of palladium mirrors rejected higher harmonics and focused the beam to maximize the flux incident on a small sample volume. Pressure was generated using a home-built, helium-membrane-controlled diamond anvil cell that allowed the sample pressure to be changed *in situ* at base temperature with better than 0.05-GPa resolution. The pressure medium was a 4:1 methanol:ethanol solution. We determined the pressure *in situ* by measuring the lattice constant of a polycrystalline silver grain included in the pressure chamber, using the Birch equation of the first kind and a low-temperature bulk modulus of 108.96 GPa (ref. 15).

The pressure cell was mounted on an X-ray compatible closed-cycle cryostat, which was in turn mounted on a precision x–y–z translation stage on the sample stage of a psi-circle diffractometer. All data presented here were measured below 8 K; for $P > 7$ GPa, all data were measured below 6 K. Our samples are miniature single crystals with typical dimensions of $100 \times 100 \times 40\ \mu m^3$ and mosaic FWHM of 0.08° at the highest measured pressure. The strict sample requirements and preparation procedures are described elsewhere[15,28]. With the focused monochromatic X-ray beam, the highly collimated diffractometer and the synchrotron flux available at beamline 4-ID-D, we achieved a sensitivity of 5×10^{-10} relative to the lattice Bragg intensity (signal one-tenth of background), which is sufficient for tracking the CDW into the quantum critical regime. For comparison of disparate CDW Bragg peaks (for example, $I(4-2Q,1,\bar{2})/I(1,1,\bar{2})$ and $I(\bar{1},3-2Q,0)/I(\bar{1},1,0)$), we converted all intensities into units of $I_{CDW} \equiv I(2Q,0,0)/I(2,0,0)$ using a procedure outlined in ref. 15; reported values of I_{CDW} include contributions from all three domain types.

Received 19 December 2008; accepted 17 March 2009.

1. de la Cruz, C. *et al.* Magnetic order close to superconductivity in the iron-based layered $LaO_{1-x}F_xFeAs$ systems. *Nature* **453,** 899–902 (2008).
2. Morosan, E. *et al.* Superconductivity in Cu_xTiSe_2. *Nature Phys.* **2,** 544–550 (2006).
3. Regal, C. A., Greiner, M. & Jin, D. S. Observation of resonance condensation of fermionic atom pairs. *Phys. Rev. Lett.* **92,** 040403 (2004).
4. Chin, C. *et al.* Observation of the pairing gap in a strongly interacting Fermi gas. *Science* **305,** 1128–1130 (2004).
5. Chen, Q., Stajic, J., Tan, S. & Levin, K. BCS-BEC crossover: from high temperature superconductors to ultracold superfluids. *Phys. Rep.* **412,** 1–88 (2005).
6. Sachdev, S. Quantum criticality: competing ground states in low dimensions. *Science* **288,** 475–480 (2000).
7. Coleman, P. & Schofield, A. J. Quantum criticality. *Nature* **433,** 226–229 (2005).
8. Nagaosa, N. Superconductivity and antiferromagnetism in high-T_C cuprates. *Science* **275,** 1078–1079 (1997).
9. Broun, D. M. What lies beneath the dome? *Nature Phys.* **4,** 170–172 (2008).
10. Fawcett, E. Spin-density-wave antiferromagnetism in chromium. *Rev. Mod. Phys.* **60,** 209–283 (1988).
11. McWhan, D. B. & Rice, T. M. Pressure dependence of itinerant antiferromagnetism in chromium. *Phys. Rev. Lett.* **19,** 846–849 (1967).
12. Yeh, A. *et al.* Quantum phase transition in a common metal. *Nature* **419,** 459–462 (2002).
13. Lee, M., Husmann, A., Rosenbaum, T. F. & Aeppli, G. High resolution study of magnetic ordering at absolute zero. *Phys. Rev. Lett.* **92,** 187201 (2004).
14. Feng, Y. *et al.* Pressure-tuned spin and charge ordering in an itinerant antiferromagnet. *Phys. Rev. Lett.* **99,** 137201 (2007).
15. Jaramillo, R. *et al.* Chromium at high pressures: weak coupling and strong fluctuations in an itinerant antiferromagnet. *Phys. Rev. B* **77,** 184418 (2008).
16. Overhauser, A. W. Spin density waves in an electron gas. *Phys. Rev.* **128,** 1437–1452 (1962).
17. Young, C. Y. & Sokoloff, J. B. The role of harmonics in the first order antiferromagnetic to paramagnetic transition in chromium. *J. Phys. F* **4,** 1304–1319 (1974).
18. Hill, J. P., Helgesen, G. & Gibbs, D. X-ray-scattering study of charge- and spin-density waves in chromium. *Phys. Rev. B* **51,** 10336–10344 (1995).
19. Pfleiderer, C. Why first order quantum phase transitions are interesting. *J. Phys. Condens. Matter* **17,** S987–S997 (2005).

20. Werner, S. A., Arrott, A. & Kendrick, H. Temperature and magnetic-field dependence of the antiferromagnetism in pure chromium. *Phys. Rev.* **155,** 528–539 (1967).
21. Rice, T. M. Band-structure effects in itinerant antiferromagnetism. *Phys. Rev. B* **2,** 3619–3630 (1970).
22. Sokolov, D. A. *et al.* Elastic neutron scattering in quantum critical antiferromagnet $Cr_{0.963}V_{0.037}$. *Physica B (Amsterdam)* **403,** 1276–1278 (2008).
23. Schroder, A., Aeppli, G., Bucher, E., Ramazashvili, R. & Coleman, P. Scaling of magnetic fluctuations near a quantum phase transition. *Phys. Rev. Lett.* **80,** 5623–5626 (1998).
24. Sweetland, E., Tsai, C.-Y., Wintner, B. A., Brock, J. D. & Thorne, R. E. Measurement of the charge-density-wave correlation length in $NbSe_3$ by high-resolution X-ray scattering. *Phys. Rev. Lett.* **65,** 3165–3168 (1990).
25. DeLand, S. M., Mozurkewich, G. & Chapman, L. D. X-ray investigation of charge-density-wave pinning in blue bronze. *Phys. Rev. Lett.* **66,** 2026–2029 (1991).
26. Gegenwart, P. *et al.* Multiple energy scales at a quantum critical point. *Science* **315,** 969–971 (2007).
27. Giamarchi, T., Rüegg, C. & Tchernyshoyov, O. Bose–Einstein condensation in magnetic insulators. *Nature Phys.* **4,** 198–204 (2008).
28. Feng, Y. *et al.* Energy dispersive X-ray diffraction of charge density waves via chemical filtering. *Rev. Sci. Instrum.* **76,** 063913 (2005).
29. Strempfer, J. *et al.* Form-factor measurements on chromium with high-energy synchrotron radiation. *Eur. Phys. J. B* **14,** 63–72 (2000).
30. Rice, T. M., Barker, A. S., Halperin, B. I. & McWhan, D. B. Antiferromagnetism in chromium and its alloys. *J. Appl. Phys.* **40,** 1337–1343 (1969).

Supplementary Information is linked to the online version of the paper at www.nature.com/nature.

Acknowledgements We are grateful to J. Pluth for assistance with sample preparation, V. Prakapenka and GeoSoilEnviroCARS (Advanced Photon Source (APS), Argonne National Laboratory) for technical support and G. Aeppli for many discussions. The work at the University of Chicago was supported by the US National Science Foundation (NSF) Division of Materials Research. GeoSoilEnviroCARS is supported by the US NSF Earth Sciences and Department of Energy (DOE) Geosciences. Use of APS is supported by the US DOE Office of Basic Energy Sciences.

Author Information Reprints and permissions information is available at www.nature.com/reprints. Correspondence and requests for materials should be addressed to T.F.R. (tfr@uchicago.edu).